Exploring pitfalls of 64Cu-labeled EGFR-targeting peptide GE11 as a potential PET tracer

Striese, F.; Sihver, W.; Gao, F.; Bergmann, R.; Walther, M.; Pietzsch, J.; Steinbach, J.; Pietzsch, H.-J.;

Originally published:

July 2018

Amino Acids 50(2018)10, 1415-1431

DOI: https://doi.org/10.1007/s00726-018-2616-5

Exploring pitfalls of ^{64}Cu-labeled EGFR targeting peptide GE11 as a potential PET tracer

Franziska Striese[1,2], Wiebke Sihver[1,*], Feng Gao[1], Ralf Bergmann[1], Martin Walther[1], Jens Pietzsch[1,2], Jörg Steinbach[1,2], Hans-Jürgen Pietzsch[1]

[1] *Helmholtz-Zentrum Dresden-Rossendorf, Institute of Radiopharmaceutical Cancer Research, Bautzner Landstraße 400, 01328 Dresden, Germany;*

[2] *Technische Universität Dresden, Department of Chemistry and Food Chemistry, 01062 Dresden, Germany*

Abbreviated title: ^{64}Cu-labeled EGFR peptides for cancer imaging

Key words: epidermal growth factor receptor, ^{64}Cu-labeled peptide conjugates, molecular imaging, receptor tyrosine kinases, positron emission tomography

***Corresponding author**: w.sihver@hzdr.de

Tel.: +49-351-260-2424

Fax: +49-351-260-3232

Acknowledgments

The authors thank Utta Herzog, Regina Herrlich and Andrea Suhr for their excellent technical assistance. The authors further wish to thank Frank Starke, Ph.D., for the synthesis and characterization of the GE11 conjugates as well as the colleagues operating at the cyclotron, Ulrike Gesche and Stefan Preusche, and the staff of the Production of Radiopharmaceuticals Department at the Institute of Radiopharmaceutical Cancer Research, Helmholtz-Zentrum Dresden-Rossendorf for the production of ^{64}Cu. F.G. thanks the German Academic Exchange Service (DAAD) for financial support (A/11/94299, 91540213). The authors also thank Ian Moore Gilpin for proofreading.

Abstract

The epidermal growth factor receptor (EGFR) represents an important molecular target for both radiotracer-based diagnostic imaging and radionuclide therapy of various cancer entities. For the delivery of radionuclides to the tumor, peptides hold great potential as a transport vehicle. With respect to EGFR, the peptide YHWYGYTPQNVI (GE11) has been reported to bind the receptor with high specificity and affinity. In the present study, GE11 with β-alanine (β-Ala-GE11) was conjugated to the chelating agent *p*-SCN-Bn-NOTA and radiolabeled with ^{64}Cu for the first radiopharmacological evaluation as a potential probe for positron emission tomography (PET)-based cancer imaging. For better water solubility, an ethylene glycol-based linker was introduced between the peptide's N-terminus and the radionuclide chelator. The stability of the ^{64}Cu-labeled peptide conjugate and its binding to EGFR-expressing tumor cells was investigated in vitro and in vivo, and then compared with the ^{64}Cu-labeled EGFR-targeting antibody conjugate NOTA-cetuximab. The GE11 peptide conjugate [^{64}Cu]Cu-NOTA-linker-β-Ala-GE11 ([^{64}Cu]Cu-**1**) was stable in a buffer solution for at least 24 h but only 50% of the original compound was detected after 24 h of incubation in human serum. Stability could be improved by amidation of the peptide's C-terminus (β-Ala-GE11-NH_2 (**2**)). Binding assays with both conjugates, [^{64}Cu]Cu-**1** and [^{64}Cu]Cu-**2**, using the EGFR-expressing tumor cell lines A431 and FaDu showed no specific binding. A pilot small animal PET investigation in FaDu tumor bearing mice revealed only low tumor uptake (standard uptake value (SUV) < 0.2) for both conjugates. The best tumor-to-muscle ratio determined was 3.75 for [^{64}Cu]Cu-**1**, at 1 h post injection. In conclusion, the GE11 conjugates in its present form are not suitable for further biological investigations, since they presumably form aggregates.

Introduction

The epidermal growth factor receptor (EGFR) is a transmembrane located receptor tyrosine kinase that regulates proliferation, differentiation or survival of cells (Wee and Wang, 2017). However, improper receptor activation may lead to a malignant cell transformation and drives cancer progression and pathogenesis. Deregulation of the receptor activity in cancer cells is mostly the consequence of activating mutations or protein overexpression (Mendelsohn and Baselga 2006). The latter has been reported for various epithelial cancers, such as head and neck, breast, prostate, bladder, colorectal, non-small cell lung cancer and glioma (Salomon et al. 1995). Moreover, EGFR overexpression often correlates with lowered overall survival and increased cancer recurrence (Selvaggi et al. 2001; Nicholson et al. 2001; Tsutsui et al. 2002). Therefore, the receptor has become an important molecular target for anticancer therapy and imaging (Sihver et al. 2014; Koi et al. 2014). Radionuclide-based molecular imaging, such as positron emission tomography (PET) can provide accurate, non-invasive and repetitive visualization of EGFR-overexpression on tumors and metastases. Moreover, it can be used for more applications, like monitor treatment responses and as a prognostic indicator for EGFR expressing tumors. For this purpose, many selective EGFR targeting ligands, from small molecular inhibitors to EGF-derived and antibody-based ligands, have been labeled with different radionuclides (Sihver et al. 2014; Yoshimoto et al. 2015; van Dijk et al. 2015)).

So far, there are few reported studies that have been conducted to image the EGFR, although more are presumably in progress (Petrulli et al. 2017; van Loon et al. 2017; Lindenberg et al. 2017). They show high accumulation in the liver with an unfavorable ratio compared to tumor accumulation. As an alternative targeting vector, peptides may be used. In the recent years, peptides became interesting radiotracers for cancer imaging since they might combine high target affinity with small molecule size, thus resulting in more favorable pharmacokinetics than antibodies. Furthermore, they are often less immunogenic (Chen and Chen 2010). Radioactive metabolites are renally eliminated relatively fast, *via* the kidneys (Bröer 2008) and, depending on the structure, not trapped in the liver. However, accumulation in the kidneys has to be monitored carefully, since they are often the dose-limiting organ for studies with radiolabeled substances. Moreover, peptides seem to be advantageous over complex proteins as they tolerate harsher conditions for radionuclide labeling (pH, temperature) and can be synthesized and manipulated more easily (Signore et al. 2001; Reubi and Maecke 2008). Because of these advantages, a number of peptide-based radiotracers have already been successfully developed for the imaging of tumors, e.g. ^{68}Ga-labeled octreotide (GaTate) targeting the somatotatin receptor as a marker of neuroendocrine tumors (Hofman et al. 2012).

Li et al., (2005) developed an EGFR-specific peptide with a 12-amino acid sequence (YHWYGYTPQNVI), by screening a phage display library with human EGFR (hEGFR). This peptide named GE11 was radioiodinated with ^{125}I at its tyrosine residues. This labeling technology potentially resulted in a mixture of three different molecules that could not be purified. The saturation binding assay showed for this mixture of ^{125}I-labeled GE11 peptides a moderate affinity of 22 nM which was determined in EGFR overexpressing cancer cells. Additionally, it has been shown that GE11 internalizes in such cells, and it can accumulate specifically in human hepatoma xenografted mice. Binding of the peptide could be displaced by EGF showing that it is specific for the EGFR. However, even though it binds into the EGF binding pocket, GE11 had only low mitogenic activity (Li et al. 2005).

Potential applications of GE11 comprises of conjugates with other larger molecules like nanoparticles, liposomes, micelles and/or with polymer compounds such as polyethylene glycol (PEG) and polyethylenimine (PEI) for the therapy of EGFR overexpressing tumors (Master et al. 2013; Cheng et al. 2014; Tang et al. 2014; Ren et al. 2015; Chanda et al.

2010; Zarschler et al. 2014; Genta et l. 2018). Radiolabeled GE11 conjugates have been already prepared with the intension of diagnostic imaging (Dissoki et al. 2011; DeJesus 2012; Yu et al. 2015; Rahmanian et al. 2017).

In the present study, approached as a proof-of-concenpt investigation, the GE11 peptide was conjugated through β-alanine with the chelator 1,4,7-triazacyclononane-1,4,7-triacetic acid (NOTA) at the peptides' N-terminus. The β-Alanine is commonly used as a spacer due to its chemical versatility for covalent conjugation (Banerjee et al. 2012). This amino acid does not have to be protected in the peptide synthesis, it prevents racemization and is useful for enantioselective synthesis (Kondo et al. 1987; Gutiérrez-Garcia et al. 2001). Additionally, an ethylene glycol (EG)-based linker was introduced to enhance the solubility in aqueous buffer. This approach should result in a chemically and stereochemically pure compound. After ^{64}Cu-labeling, radiopharmacological investigations of the peptide conjugates were performed with regard to cell binding in vitro, as well as biodistribution and accumulation in tumors from the head and neck squamous cell carcinoma (HNSCC) cell line FaDu in xenografted mice in vivo. The focus of the project was to develop a diagnostic imaging tool, particularly for HNSCC, since elevated EGFR expression in such entities have been associated with poor clinical prognosis and resistance to chemotherapy and radiation therapy (Ang et al. 2002; Baumann and Krause 2004; Martinez-Useros and Garcia-Foncillas 2015). Hence, the moderately high EGFR expressing HNSCC cell line FaDu was used, especially for xenografting. Thus, the potential of the peptide conjugates as candidates for further application as diagnostic PET tracers was intended to be estimated and finally compared with the EGFR-targeting antibody conjugate, ^{64}Cu-radiolabeled NOTA-cetuximab.

Materials and Methods

Chemicals and equipment

Chemical reagents and solvents were purchased from commercial sources, without further purification. *p*-SCN-Bn-NOTA was purchased from Macrocyclics (Dallas, TX, USA), LiChrolut®RP-18 cartridges from Merck Millipore Group (Darmstadt, Germany) and Jumbo- or Macrosep centrifugal devices with a molecular weight cut-off (MWCO) of 30 kDa were received from Pall Corporation (Ann Abor, MI, USA). The EG-based linker (cf. Fig. 1) was prepared in-house (Heldt et al. 2013).

β-Alanine-YHWYGYTPQNVI (β-Ala-GE11) and β-Alanine-YHWYGYTPQNVI-NH_2 (β-Ala-GE11-NH_2) were purchased from GL Biochem (Shanghai, China). Cetuximab (Erbitux®, C225) was purchased from Merck Serono (Darmstadt, Germany).

HPLC was carried out with an HPLC system of Knauer (Berlin, Germany), equipped with a Smartline 2800 UV/Vis-detector and, for radiochemical analysis, a flow-through radioactivity detector Ramona from Raytest GmbH (Straubenhardt, Germany). Knauer Eurospher 100 C18 columns (5 µm, X × 250 mm) with an inner diameter of either 4 mm or 8 mm were used for analysis or purification of the GE11 peptide conjugates, respectively. For these columns the mobile phase consists of water (**A**) and acetonitrile (AcN) + 0.1% trifluoroacetic acid (TFA) (**B**); the flow was 1 mL/min. A YMC-BioPro QA-F column (5 µm, 4.6 × 100 mm) was used for analytical HPLC of $NOTA_3$-C225. Here, the mobile phase was composed of 20 mM Tris/HCl (pH 8.5) (**A**) and 1 M NaCl in 20 mM Tris/HCl (pH 8.5) (**B**) with a 0.35 mL/min flow.

Matrix-assisted-laser desorption/ionization – time of flights mass spectrometry (MALDI-TOF-MS) was carried out with a *Daltonic Autoflex II* TOF/TOF mass spectrometer from Bruker Daltonics (Bremen, Germany) and 0.1 M sinapinic acid

(3-(4-hydroxy-3,5-dimethoxyphenyl)prop-2-enoic acid) as a matrix, which was dissolved in a mixture of AcN, ddH_2O (60/40 (v/v)) and 0.1% TFA.

The ^{64}Cu ($t_{½}$ = 12.7 h) production was performed at the Helmholtz-Zentrum Dresden-Rossendorf with a Cyclone 18/9 cyclotron (IBA, Louvain la Neuve, Belgium) *via* the $^{64}Ni(p,n)^{64}Cu$ reaction. Radioactive samples were counted using a 1480 WIZARD 3″ automatic gamma counter from PerkinElmer (Waltham, USA).

Cell culture reagents were obtained from Biochrom GmbH (Berlin, Germany).

Synthesis of GE11 and C225 conjugates

β-Ala-GE11 and β-Ala-GE11-NH_2. Both peptides comprised an additional β-alanine at the N-terminus for conjugation reactions (Fig. 1A).

NOTA-β-Ala-GE11. β-Ala-GE11 (5.58 µmol) and triethylamine (TEA, 55.8 µmol) were dissolved in anhydrous dimethylformamide (DMF). A solution of *p*-SCN-Bn-NOTA (5.58 µmol) in anhydrous DMF (700 µL) was added and the reaction mixture shaken over night (o/n) at room temperature (RT). The pale yellow solution was finally purified by HPLC (gradient from **A**: 75% to 64% in 20 min: retention time (t_R)= 12.9 min) and the product freeze-dried obtaining a white solid with a chemical yield of 37%. MALDI-TOF *m/z*: 2062.9 $[M+H]^+$ (expected mass: 2062.3).

linker-β-Ala-GE11, linker-β-Ala-GE11-NH_2. The EG-based linker precursor (8 µmol) and the coupling reagent CoMu (8 µmol) were dissolved in anhydrous DMF (500 µL). β-Ala-GE11 or β-Ala-GE11-NH_2 (8 µmol), and diisopropylethylamine (80 µmol) in anhydrous DMF (500 µL) were added to the linker precursor. The reaction mixture was shaken o/n at RT. After addition of piperidine (2 mL) and anhydrous DMF (1 mL), the reaction mixture was stirred for 1 h at 40 °C. The solvents were removed on a rotary evaporator and the residual yellowish oil purified by HPLC (gradient from **A**: 80% to 67% in 25 min: linker-GE11 t_R= 18.7 min, linker-GE11-NH_2 t_R = 21.1 min). After freeze-drying, both peptides were obtained as white solids with chemical yields of 38% and 53%, respectively. MALDI-TOF *m/z*: 1861.5 $[M+2H]^+$ (expected mass: 1858) (linker-β-Ala-GE11), MALDI-TOF *m/z*: 1858 $[M+H]^+$ (expected mass: 1857) (linker-β-Ala-GE11-NH_2).

*NOTA-linker-β-Ala-GE11 (=**1**), NOTA-linker-β-Ala-GE11-NH_2 (=**2**).* (Fig. 1B) linker-β-Ala-GE11, or linker-β-Ala-GE11-NH_2 (1 µmol), and TEA (1 µmol) were dissolved in anhydrous DMF (300 µL). A solution of *p*-SCN-Bn-NOTA (1 µmol) in anhydrous DMF (300 µL) was added and the reaction mixture shaken o/n at RT. The pale yellow solution was purified by HPLC (gradient from **A**: 80% to 60% in 30 min: **1** t_R= 20.5 min, **2** t_R= 21.2 min). After freeze-drying, **1** and **2** were obtained as white solids with chemical yields of 62% and 63%, respectively. MALDI-TOF *m/z*: 2308.1 $[M+H]^+$ (expected mass: 2307) (**1**), 2309.2 $[M+H]^+$ (expected mass: 2308) (**2**).

$NOTA_3$-C225. The C225 solution (8 mL, 5 mg/mL, 40 mg, 263.2 nmol) was buffer exchanged using centrifugal filter units with a 30 kDa MWCO for a $NaHCO_3$ buffer (55 mL, 50 mM containing 0.9% NaCl, pH 6.4) and concentrated to a final volume of 3.5 mL. *p*-SCN-Bn-NOTA (27.3 mg, 49 µmol) was dissolved in a HEPES buffer (0.5 M, 2 mL, pH 7.2) and added dropwise to the buffer-exchanged C225 solution, which was then filled up to 6.89 mL with the HEPES buffer (molar ratio *p*-SCN-Bn-NOTA:C225 185:1) obtaining pH 6.9. After 22 h at RT, the modified C225 solution was purified from unbound *p*-SCN-Bn-NOTA, again using centrifugal filter units with a 30 kDa MWCO and a $NaHCO_3$ buffer (55 mL, 50 mM containing 0.9% NaCl, pH 6.4) and concentrated to a final volume of 1 mL. The yield of $NOTA_3$-C225 was determined by UV/Vis spectroscopy at 280 nm, resulting in 260 nmol (99%). HPLC (gradient from **A**: 100% to 0% in 20

min: t_R = 5.1 min). The identification of the final product and the number of coupled NOTA chelator molecules was confirmed by MALDI-TOF (*m/z*: 154106.6 $[M+H]^+$) (Schubert et al. 2017).

A -NH-Tyr-His-Trp-Tyr-Gly-Tyr-Thr-Pro-Gln-Asn-Val-Ile-OH (GE11)

-NH-Tyr-His-Trp-Tyr-Gly-Tyr-Thr-Pro-Gln-Asn-Val-Ile-NH_2 (GE11-NH_2)

B

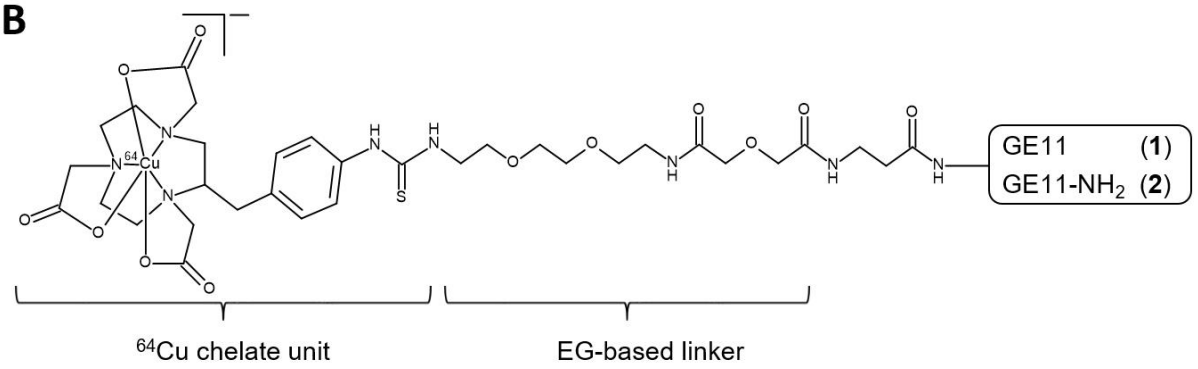

Fig. 1 (**A**) Amino acid sequences of GE11 and GE11-NH_2, (**B**) [^{64}Cu]Cu-**1** and [^{64}Cu]Cu-**2**

Radiolabeling of the peptide conjugates and $NOTA_3$-C225

The ^{64}Cu-labeling of the **1** or **2** conjugate was conducted as follows: 2-(N-morpholino) ethanesulfonic acid (MES) buffer (0.2 M, 100 µL, pH 6.2) was mixed with the peptide conjugate (until 10 µM). Thereafter, up to 50 MBq [^{64}Cu]$CuCl_2$/0.01 M HCl were added to the peptide conjugate-MES solution. The reaction was supplemented with water to a final volume of 400 µL. After shaking the reaction vial (polypropylene vials, Eppendorf) for 1 h at 50 °C, the radiochemical purity was monitored by HPLC (gradient from **A**: 90% to 10% in 20 min).

([^{64}Cu]Cu-NOTA)$_3$-C225 was prepared by first buffering the [^{64}Cu]$CuCl_2$/0.01 M HCl (50 to 80 MBq) solution with one equivalent volume of a MES-buffer (1 M, pH 6.0). Then, $NOTA_3$-C225 (0.5 nmol) was added to a MES-buffer (0.1 M, pH 6.0). Both solutions were mixed and incubated for 45 min at 30 °C. Then, a 6-fold molar excess of ethylenediaminetetraacetic acid (EDTA) was added and incubated for a further 15 min at RT. The radiochemical purity was determined by radio-instant thin layer chromatography (iTLC) using ITLC-SA plates (Agilent Technologies, Santa Clara, CA, USA) and water as the mobile phase. The Rita-Star image reader (Raytest GmbH, Germany) was used for the analysis of the plates.

Octanol/buffer partition coefficient (LogD). 20 µL of [^{64}Cu]Cu-**1** or [^{64}Cu]Cu-**2** (0.2 MBq) was diluted into 500 µL of PBS. 500 µL of n-octanol was added and the mixture stirred for 30 min at RT. Subsequently, the mixture was centrifuged for 30 min (14,000*g*) at RT; 450 µL of both water and n-octanol phases were taken and centrifuged again. The activity of 100 µL of both the buffer phase and the octanol phase was measured in a gamma counter and the Log*D* was calculated. The experiments were performed three times.

In vitro characterization

Stability in human serum, cell medium and MES-buffer. The integrity of the ^{64}Cu-labeled peptide conjugates was evaluated for the following media: human serum, cell culture medium DMEM + 10% fetal calf serum (FCS) (with (w/) and without (w/o) the presence of A431 cells) and 0.2 M MES-buffer pH 6.2. The incubation took 2 h and 24 h at 37 °C,

respectively. Conjugate degradation was monitored by analytical HPLC. Before HPLC analysis, the conjugates were extracted from the biological fluid with a LiChrolut® RP18 cartridge. The peptides were eluted from the cartridge with AcN/ddH_2O (80/20 (*v/v)*), which was subsequently evaporated to dryness. Then, the conjugate peptides were dissolved in a MES-buffer (100 µL, 0.2 M, pH 6.2) and applied to the HPLC column (gradient from **A** (water): 90% to 10% in 20 min, (**B**: AcN + 0.1% TFA)). A small part of [^{64}Cu]Cu-**1** and [^{64}Cu]Cu-**2** was kept for MALDI-TOF-MS analysis. The HPLC radioflow-peak areas were measured by employing manual peak integration. The remaining portion of the parent compound was calculated by determining the area of the parent radioflow-peak as a percentage of the total area of all peaks. For mass determination, the solution was again evaporated. The measurements resulted in *m/z*: 2370.2 $[M+H]^+$ (parental peptide Cu-**1**, expected mass 2369), 2369.3 $[M+H]^+$ (parental peptide Cu-**2**, expected mass 2368); for both peptides 1899.7 $[M+H]^+$ (Cu-NOTA-linker-β-Ala-Tyr-His-Trp-Tyr-Gly-Tyr-Thr-Pro, expected mass 1899), 1542.5 $[M+H]^+$ (Cu-NOTA-linker-β-Ala-Tyr-His-Trp-Tyr-Gly, expected mass 1539). The experiment was repeated at least twice for each peptide conjugate.

Cell assays

The cell culture assays were assessed using the highly EGFR expressing human epidermoid carcinoma cell line A431 (2.6 Mio EGFR/cell; Haigler et al. 1978) (ATCC® CRL-1555), the moderately highly EGFR expressing HNSCC cell line FaDu (0.24 Mio EGFR/ cell; Schütze et al 2007) (ATCC®HTB-43) and, as a control, the non-EGFR expressing human melanoma cell line MDA-MB435s (ATCC®HTB-129). The cells were grown as a monolayer up to confluence at 37 °C in a humidified atmosphere comprising of 5% CO_2 in a DMEM medium supplemented with 10% FCS.

Verification of EGFR protein levels for A431, FaDu and MDA-MB-435s cells. Whole cell lysates were prepared and the protein concentration of each sample was determined by the bicinchoninic acid (BCA) protein assay kit (see below). Equal amounts of denatured protein (3 µg) were separated by SDS-PAGE (with 10% separating gel) and subsequently transferred onto a polyvinylidene fluoride (PVDF) membrane. The membrane was blocked with 5% bovine serum albumin (BSA) in Tris-buffered saline + 0.1% Tween® 20 (TBST) for 1 h, followed by a 1 h-incubation with appropriate primary antibodies (rabbit anti-EGFR 1:10000; rabbit anti-β-actin 1:5000, New England Biolabs; Frankfurt am Main, Germany) diluted with 5% BSA in TBST. After washing three times in TBST, the blots were incubated with a horseradish peroxidase (HRP)-conjugated secondary antibody (goat anti-rabbit-HRP 1:40000, New England Biolabs) for 1 h in 5% BSA-TBST. The visualization of the HRP-enzyme activity was accomplished with Western blotting luminol reagent according to manufacturer's instructions (Santa Cruz Biotechnology, Dallas, TX, USA). Enhanced chemiluminescence was detected with an imaging system suitable for chemiluminescent Western blots (Stella 2000, Raytest).

Viability assay. Standard MTS (3-(4,5-dimethylthiazol-2-yl)-5-(3-carboxymethoxy-phenyl)-2-(4-sulfophenyl)-2H-tetrazolium)-assay (CellTiter 96® AQueous One Solution Cell Proliferation Assay, Promega, Madison, WI, USA) was performed in order to study the growth influence of β-Ala-GE11 (1.3 µM to 130 µM) in comparison with C225 (0.7 nM to 330 nM) in A431 and FaDu cells. The method was performed according to the manufacturer's protocol. Absorption at a wavelength of 492 nm was recorded by Sunrise™ microplate reader (Tecan Group, Männedorf, Switzerland). As control for viability termination cell samples were treated with 0.1% of Triton X-100.

Saturation binding assays on cell homogenate. To avoid ligand-receptor internalization, cell homogenate was prepared. After detaching from the culture dish, cells were centrifuged for 5 min at 600*g* and the pellets subsequently stored at -80 °C until usage. For an assay, pellets were thawed in medium and homogenized with a homogenizer (Potter-Elvehjem) by 20 strokes on ice.

For saturation assays, cell homogenate was exposed to varying concentrations of [^{64}Cu]Cu-**1**/**2** (0.4 to 50 nM, molar activities of 5 to 10 GBq/µmol) and for comparison with the standard EGFR ligand ([^{64}Cu](Cu-NOTA)$_3$-C225 (0.2 to 20 nM, molar activities of 50 to 100 GBq/µmol) for 1 h at 4 °C and 37 °C, respectively. Adjacent samples additionally received 50 µM β-Ala-GE11, β-Ala-GE11-NH_2 or 0.33 µM C225 to assess the nonspecific binding. The incubation was terminated by filtration through GF/C Whatman filters (treated with 0.3% PEI for at least 90 min) using a harvester (Brandel, Glasgow, UK). After washing the filters four times with ice-cold phosphate buffered saline (PBS), they were punch-transferred into vials and counted in a gamma counter. To determine adhered activity to the incubation vials, the PBS washed vials also were measured in the gamma counter.

Saturation binding and displacement assays in intact cells. Cells were seeded at a density of 1.5×10^5 cells/well (48-well plates). After 24 h for attaching, the cells were washed twice with 500 µL PBS. To reduce the nonspecific binding at the plastic device, the culture dishes were blocked with 500 µL of 10 g/L BSA in PBS for 1 h. Then, incubation with the radioligand and determination of nonspecific binding was performed as describe above for the homogenate procedure. For competition studies, A431 cells first received up to 1 mM of either β-Ala-GE11 or β-Ala-GE11-NH_2, up to 1 µM of EGF or up to 0.33 µM of C225 at 4 °C and 37 °C for 1 h. Then, ([^{64}Cu](Cu-NOTA)$_3$-C225 (1 nM) was added for another hour. The incubation was terminated by aspirating the binding medium, after which the cells were rinsed thrice with ice-cold PBS to remove any unbound radioligand. Finally, the cell monolayer was dissolved by incubating them with 1 mL cell lysis buffer (0.1 M NaOH and 1% SDS) for 30 min at RT. 500 µL of the cell lysate were used to quantify the activity of cell-bound ligand in the gamma counter. To measure radioligand binding only to the plastic device, an identical saturation binding assay was conducted without cells.

The protein concentration of cell samples (homogenate and intact cell assay) was determined by the BCA protein assay kit (Pierce™ Thermo Scientific; Waltham, MA, USA) according to manufactures' instruction measuring the absorbance of the protein color complex at 562 nm with a spectrophotometer (Multimode Reader Varioscan™Flash, Thermo Scientific) in comparison to a BSA standard curve.

The binding data were calculated by performing nonlinear curve fitting with GraphPad Prism 5.03.

EGF-displacement using immunoblotting analysis. The assay was performed to find out in a different way, whether GE11, as compared to C225, can be displaced by EGF and thus prevent the phosphorylation of the EGFR. 5000 A431 cells/well were seeded into a flat bottom 12-well plate. After 48 h, the medium was replaced by DMEM (500 µL) and incubated for further 24 h in the incubator. Then, the serum-starved cells were treated with or without 0.1 and 1 mg/mL β-Ala-GE11, 10 and 100 µg/mL C225 or vehicle controls for 4 h at 37 °C. Thereafter, the cells were stimulated with 0.1 µg/mL of EGF for 15 min or left unstimulated. Following, cell lysis, sample preparation, SDS-PAGE and Western blotting were conducted equivalent to the procedures in the section: *Verification of EGFR protein levels*. Then, an immunostaining was performed with rabbit anti-phosphorylated-EGFR(Y1173) (1:2500, New England Biolabs) diluted in 5% BSA in TBST or rabbit anti-β-actin as primary antibodies and goat anti-rabbit-HRP as secondary antibody. After detection, the primary and secondary antibodies were removed from the PVDF membrane by stripping (0.1 M NaOH, 0.5% dithiothreitol, 2% SDS) for 15 min at 55 °C. The membrane was subsequently washed twice with TBS for 5 min and a second immunostaining was conducted as described in *Verification of EGFR protein levels* with rabbit anti-EGFR and rabbit anti-βactin as primary antibodies and goat anti-rabbit-HRP as secondary antibody.

Animal experiments

Male Wistar rats (aged 5 to 6 weeks, 200 ± 11 g; Harlan Winkelmann GmbH, Borchen, Germany) and female NMRI *nu/nu* mice (aged about 11 weeks; Experimental Centre of the Medical Faculty Carl Gustav Carus, Technische Universität, Dresden, Germany) were kept under standard conditions with free access to food and water. For blood drawing venous catheters were placed.

To establish the FaDu xenograft model small pieces from source tumors of human hypopharyngeal carcinoma FaDu were engrafted into the right hind-leg of mice under desflurane anesthesia (8-10% desflurane, 30% oxygen/air) (Schubert et al. 2017).

Biodistribution. Investigation of biodistribution of ^{64}Cu-radiolabeled peptide conjugates followed a protocol published elsewhere with some modifications (Bergmann et al. 2013). In brief, 8 rats received injections into a lateral tail vein under anesthesia (inhalation of 9-10% desflurane (Suprane, Baxter, Germany) in 30% oxygen/air (gas flow 0.5 L/min)). The injection volume of either [^{64}Cu]Cu-**1** or [^{64}Cu]Cu-**2** (0.5 MBq/animal; radiochemical purity of >98%; specific activity 0.2 to 1 MBq/µg, molar activity 0.5 to 2.3 GBq/µmol), dissolved in electrolyte solution E-153 (Serumwerk Bernburg, Germany)), pH 7.2, was 0.5 mL. Biodistribution was determined in groups of four rats (per time point) sacrificed by heart puncture under anesthesia at 5 min and 60 min post injection (p.i.). Organs and tissues of interest (blood, brain, brown adipose tissue (BAT), white adipose tissue (WAT), thyroid gland, thymus, harderian glands (Harderian.gl.), heart, lungs, muscle, pancreas, skin, spleen, femur, testes, adrenals, kidneys, liver, intestine and stomach) were rapidly excised, weighed, and the activity determined in a Wallac WIZARD Automatic Gamma Counter and a dose calibrator (dose calibrator ISOMED 2000, MED Nuklear-Medizintechnik Dresden GmbH, Dresden, Germany), respectively. The activity of ^{64}Cu in the tissue samples was decay-corrected and calibrated by comparing the counts in tissue with the counts in aliquots of injected radiotracer that have been measured both in the gamma counter and the dose calibrator and at the same time. The activity concentration in organs and tissues was calculated as standardized uptake value (SUV = (activity in the organ / weight of the organ) / (injected activity / animal weight)). The accumulated activity %ID was calculated for all fully extractable organs. The intestine and stomach were measured with content (w.c.) and urine activity was calculated as the difference between the activity recovery and the injected activity.

For investigation of blood clearance and metabolic stability, blood samples were taken at 1, 3, 5, 10, 20, 30 und 60 min p.i. and measured in a gamma counter. For in vivo stability, the percentage of intact radiolabeled compound was determined via HPLC, 0, 1, 3, 10, 20 and 30 min after injection of [^{64}Cu]Cu-**1** or [^{64}Cu]Cu-**2** (Fig S1).

Small animal PET. ^{64}Cu-labeled GE11 conjugates **1** and **2** (10 to 20 MBq) of high molar activity (400 to 700 GBq/µmol) and ([^{64}Cu]Cu-NOTA)$_3$-C225 (20 MBq, molar activity 50 to 100 GBq/µmol) were injected into the tail vain of FaDu tumor bearing mice kept under general desflurane anesthesia. The PET studies were performed over a period of 1 h ([^{64}Cu]Cu-**1** or [^{64}Cu]Cu-**2**) and 36 h ([^{64}Cu]Cu-NOTA)$_3$-C225) with a small animal PET scanner (micro PET® P4, Siemens medical solutions, Knoxville, TN, USA). The emission data were reconstructed, random coincidences subtracted and the detector efficiencies were normalized using the producer's software. The ROVER software (ABX GmbH, Radeberg, Germany) was used for data evaluation. The injected dose was calculated from the activity difference of the syringe before and after injection having been measured with a cross calibrated dose calibrator. The data were used to calculated SUV (SUV for PET: averaged activity concentration in a region of interest (ROI) / injected activity × animal weight).

Of note, the approved animal experiments (reference number 24-9168.21-4/2004-1) a priori were planned as an orientation survey (pilot study) to at least prove the harmlessness of a novel (radioligand) potential of radiotracers in the interest of (radio)pharmaceutical drug safety.

Results

Preparation, radiochemical characterization and stability of the conjugates

The GE11 peptide was obtained commercially with an additional β-alanine at the N-terminus, in order to allow coupling of the chelating agent *p*-SCN-Bn-NOTA. The purity of the peptide conjugate was higher than 99% verified with analytical HPLC, and characterized by MALDI-TOF/TOF mass spectrometry. However, the EG-linkerfree conjugated NOTA-derivative was not soluble in aqueous buffer, only with addition of an organic solvent like ethanol (> 20%). Therefore, a hydrophilic EG-based linker molecule was introduced between the N-terminus of the peptide and the chelator (Fig. 1A,B). For coupling with the GE11 peptide at the N-terminus the linker precursor contained a Fmoc protected amino group and a reactive free carboxylic group. The *p*-SCN-Bn-NOTA was coupled with the deprotected linker-amino group. The in vitro stability of the ^{64}Cu-labeled peptide conjugate **1** was investigated in 0.2 M MES buffer (pH 6.2) and in cell medium DMEM + 10% FCS (w/ and w/o A431 cells) (Table **1**). Further, the stability in human blood serum and binding of human serum components in vitro was determined. Whereas the stability in buffer and cell medium was excellent high after 24 h with more than 95% for the radiolabeled peptide **1**, the stability decreased in human blood serum within 24 h to only about 50% of parental compound. MALDI-TOF mass analysis was used for the investigation of degradation products upon incubation with human serum. With this method, the parenteral compound and two metabolites were detected, with masses that correspond to following cleavage products: 2370.2 $[M+H]^+$ (Cu-**1**), 1899.7 $[M+H]^+$ (Cu-NOTA-linker-β-Ala-Tyr-His-Trp-Tyr-Gly-Tyr-Thr-Pro), 1542.5 $[M+H]^+$ (Cu-NOTA-linker-β-Ala-Tyr-His-Trp-Tyr-Gly).

The mass data might indicate an exopeptidase-mediated cleavage with begin at the free C-terminus of the peptide. One conventional method to prevent proteolytic cleavage is to protect the C-terminal carboxyl group by amidation (Di 2015). Thus, β-Ala-GE11-NH_2 was conjugated to the linker and the NOTA chelator similar to **1** to obtain **2** (Fig. 1A,B). The stability of [^{64}Cu]Cu-**2** in human blood serum was improved resulting in ≥ 70% unmetabolized product after 24 h.

The octanol/buffer partition coefficient (Log*D*) determination with the shake-flask method yielded values -3.81 and -3.32 for the ^{64}Cu-labeled conjugate **1** and **2**, respectively (Table **1**).

In vitro cell assays

The NOTA-conjugated peptides **1** and **2** were labeled with ^{64}Cu with a radiochemical purity > 95% (as determined radio-HPLC). For the in vitro assays, the molar activities of [^{64}Cu]Cu-**1** and [^{64}Cu]Cu-**2** ranged between 5 and 25 GBq/µmol at the end of radiolabeling procedure, whereas for the in vivo studies [^{64}Cu]Cu-**1** and [^{64}Cu]Cu-**2** were obtained with higher molar activities up to 700 GBq/µmol. The radiometric HPLC analysis of [^{64}Cu]Cu-**1** and [^{64}Cu]Cu-**2** is presented in Fig. 2. For both peptides a single peak (with a very weak shoulder in Fig. 2A) was observed at a retention time of 11.5 and 11.8 min, respectively, whereas the peak for free [^{64}Cu]$CuCl_2$ already appeared at 2.7 min.

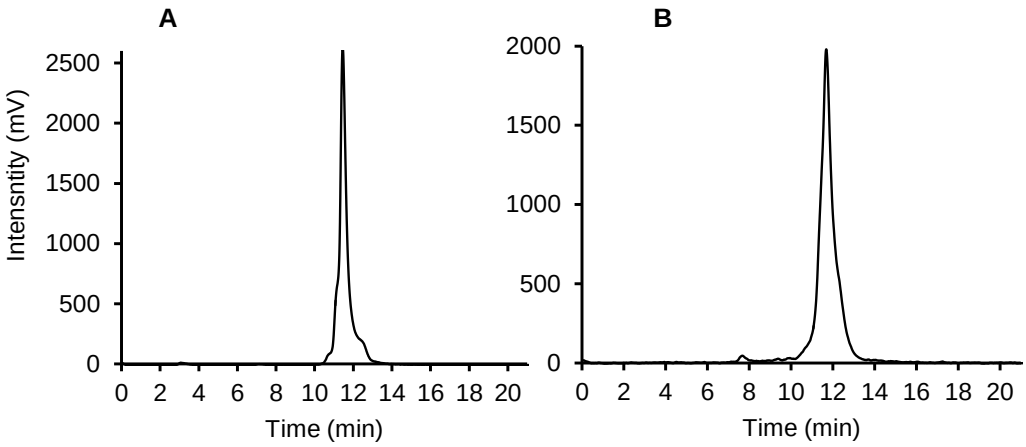

Fig. 2 Analytical radio-HPLC chromatogram of (**A**) [^{64}Cu]Cu-**1** (t_R = 11.5 min) and (**B**) [^{64}Cu]Cu-**2** (t_R = 11.8 min).

Table 1 Log*D* of the radiolabeled conjugates as well as stability in 0.2 M MES buffer (pH 6.2), in human blood serum, and in cell medium w/ and w/o A431

	Time	[^{64}Cu]Cu-**1**	[^{64}Cu]Cu-**2**
Log*D*		-3.81 ± 0.06	-3.32 ± 0.03
0.2 MES buffer (pH 6.2)	2 h	≥ 99%	≥ 96%
	24 h	≥ 97%	≥ 97%
Human blood serum	2 h	≥ 93%	≥ 98%
	24 h	≥ 50%	≥ 70%
DMEM w/ A431, w/ 10% FCS	1 h	≥ 94%	≥ 95%
	24 h	≥ 94%	≥ 92%
DMEM w/o A431, w/ 10% FCS	1 h	≥ 98%	≥ 95%
	24 h	≥ 98%	≥ 95%

Tests were performed at 37 °C, at least three independent experiments

Cell assays

The immunologic detection of protein levels for the EGFR in A431, FaDu and MDA-MB-435s cells is demonstrated in Fig. 3 showing the abundance of endogenously expressed receptor protein: high for A431, moderate for FaDu and no detectable EGFR protein for MDA-MB-435s.

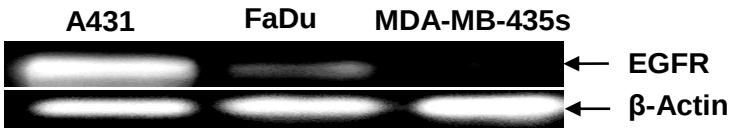

Fig. 3 Detection of endogenous EGFR expression of A431, FaDu and MDA-MB-435s (negative control) cells relative to β-actin expression by Western blotting

The influence of β-Ala-GE11 compared to C225 on the viability of A431, FaDu and MDA-MB-435s cells was investigated by applying the MTS test. Treatment with the peptide conjugates even at concentrations of 130 µM did not notably influence the viability of the three cell lines after 24 h (Fig. 4 A). In contrast, treatment with only 330 nM C225

tended to decrease the viability of FaDu and A431 cells after 24 h whereas on MDA-MB-435s cells the viability did not change (Fig. 4 B).

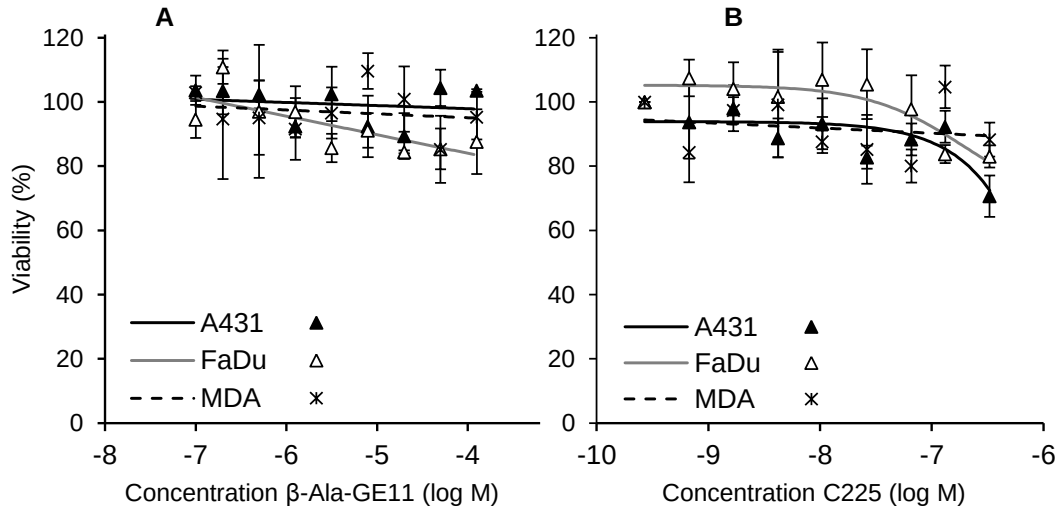

Fig. 4 Effects of (**A**) β-Ala-GE11 and (**B**) C225 treatment on the viability of A431 (solid black line, black triangles), FaDu (solid gray line, empty triangles) and MDA-MB435s cells (dashed black line, asterisks) after 24h. Results are expressed as percentages of the untreated medium control value. Each data point represents the mean from two to four experiments ± SEM

Saturation binding assays were performed to determine the binding affinity of ^{64}Cu-labeled peptide conjugates **1** and **2**. Initially, the experiments were conducted on cell homogenates with a cell harvester that uses a filter to trap the cell membrane. However, [^{64}Cu]Cu-**1** or **2** resulted not in any specific binding for A431, FaDu as well as for MDA-MB-453s cells. Instead, saturation assays with established standard conjugate ([^{64}Cu]Cu-NOTA)$_3$-C225 showed moderate to high affinity on A431 and FaDu cell homogenate: K_d 8.5 ± 3.6 nM and 0.6 ± 0.1 nM, respectively. The B_{max} was 63.8 ± 9.4 pmol/mg and 4.8 ± 0.5 pmol/mg protein for A431 and FaDu homogenate, respectively (Fig. 5A,B). For MDA-MB-453s cells hardly any specific binding could be determined with ([^{64}Cu]Cu-NOTA)$_3$-C225 (Fig. 5C). At 4°C the K_d value for A431 was higher (18 ± 3), but B_{max} did not change; and for FaDu homogenate similar binding data were obtained.

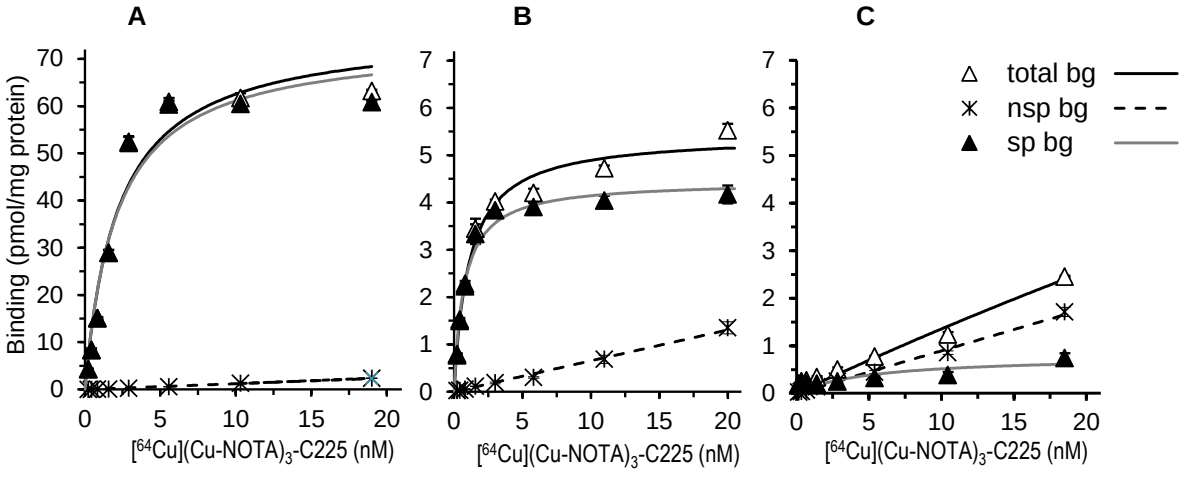

Fig. 5 Binding curves of ([^{64}C]Cu-NOTA)$_3$-C225 from saturation assays on (**A**) A431, (**B**) FaDu and (**C**) MDA-MB-453s (negative control) cell homogenate at 37 °C. The curves comprise data of one representative assay from a total of four independent assays. (Empty triangle, black line: total binding; asterisks, dotted line: nonspecific binding; black triangle, gray line: specific binding)

Closer to natural conditions is the incubation of the radiolabeled peptides on intact cells direct in the growing wells. Again, saturation assays using [^{64}Cu]Cu-**1** or **2** on intact cell condition did not show analyzable specific binding neither for A431 nor for FaDu and also not for the negative control cell line MDA-MB-453s (Fig. 6). For ([^{64}Cu]Cu-NOTA)$_3$-C225 the K_d-values were 8.3 ± 1.5 nM (A431) and 0.9 ± 0.2 (FaDu) and the B_{max} was 17.7 ± 1.5 (A431) and 1.3 ± 0.1 pmol/mg protein (FaDu) at 4 °C. At 37 °C, the values for A431 cells differ clearly from those measured at 4 °C with a K_d 37.1 ± 8.6 nM and B_{max} 56.6 ± 9.6 pmol/mg protein, whereas the values for FaDu cells were almost similar with a K_d 0.7 ± 0.1 nM and B_{max} 2.7 ± 0.1 pmol/mg protein.

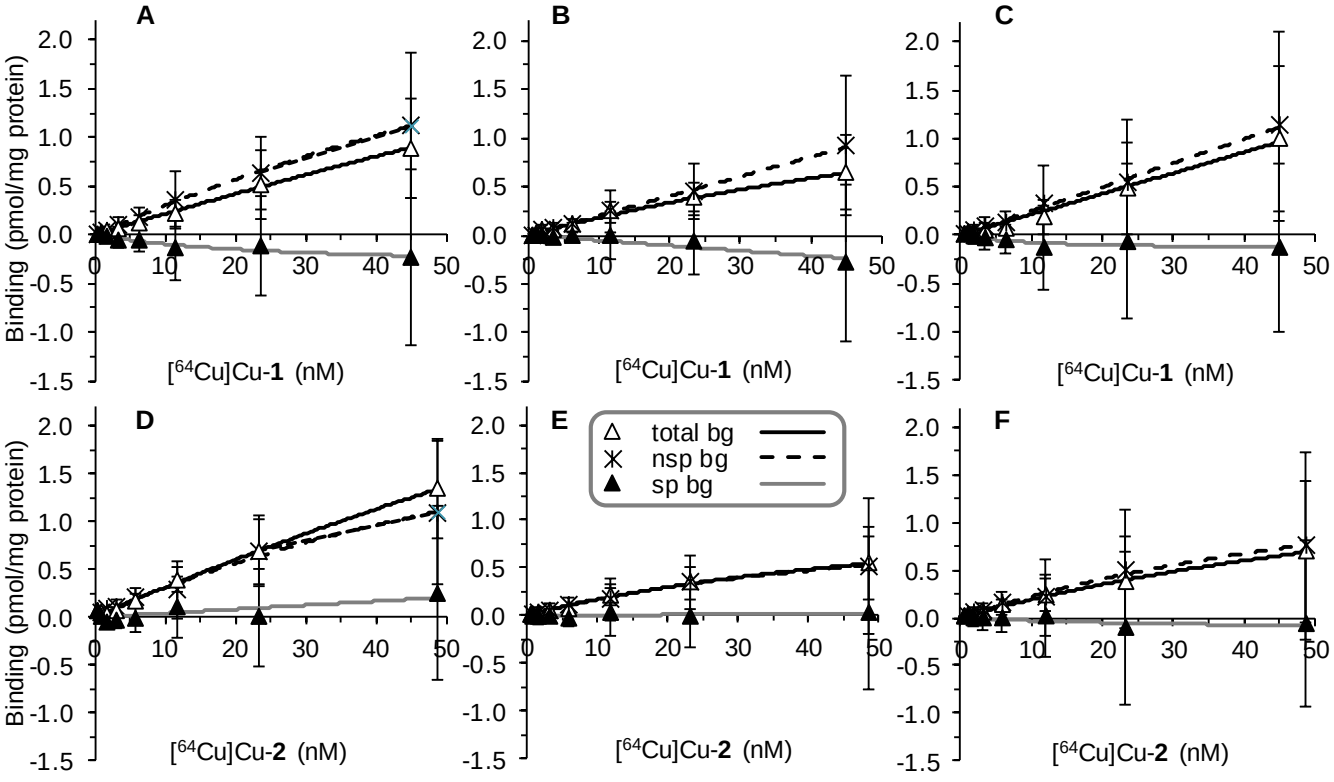

Fig. 6 Binding curves of [^{64}Cu]Cu-**1** (upper row) and [^{64}Cu]Cu-**2** (lower row) from saturation assays on (**A**,**D**) A431, (**B**,**E**) FaDu and (**C**,**F**) MDA-MB-453s on intact cells at 37°C. The curves comprise data of two independent assays. (Empty triangle, black line: total binding; asterisks, dotted line: nonspecific binding; black triangle, gray line: specific binding)

In the competition assay on A431 cells, increasing C225 concentration caused a progressive displacement of the ([^{64}Cu]Cu-NOTA)$_3$-C225 from its EGFR binding sites (Fig. 7A). The unlabeled antibody was able to displace ([^{64}Cu]Cu-NOTA)$_3$-C225 completely upon an 100-fold excess. The affinity at 4 °C and 37 °C was almost similar with K_i-values for C225 of 2.1 and 1.6 nM for 4 °C and 37 °C, respectively. ([^{64}Cu]Cu-NOTA)$_3$-C225 binding was also reduced with increasing EGF concentration (Fig. 7B). However, EGF could not completely displace ([^{64}Cu]Cu-NOTA)$_3$-C225 from the EGFR. The rate of displacement and EGF-binding affinity was temperature-dependent. At 37 °C, ([^{64}Cu]Cu-NOTA)$_3$-C225 could be displaced more efficiently and the affinity of EGF was higher (K_i 16 nM) than at 4 °C (K_i 58 nM). In contrast, β-Ala-GE11 had no effect on binding of ([^{64}Cu]Cu-NOTA$_3$)-C225 even at an excess of 1×10^6 with respect to the applied molar concentration (Fig. 7C).

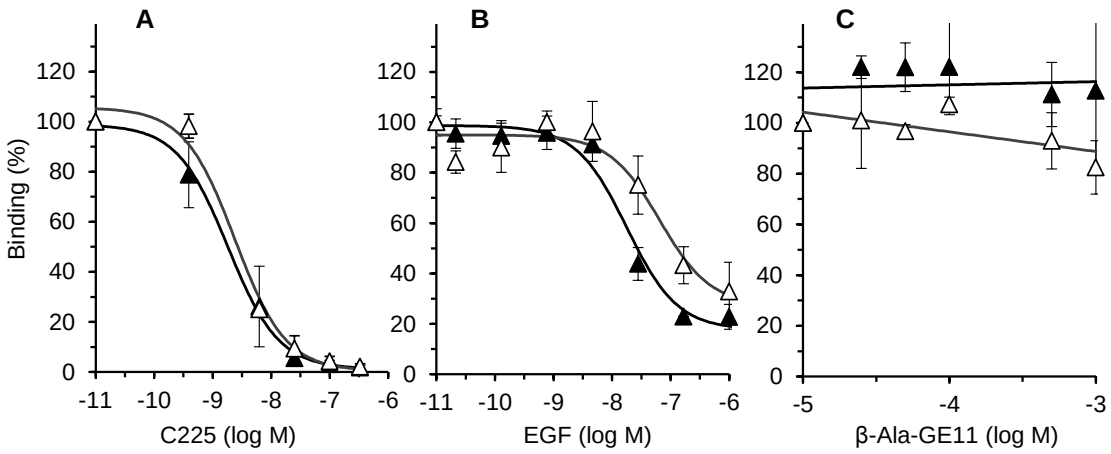

Fig. 7 Displacement assays with (**A**) C225, (**B**) EGF and (**C**) β-Ala-GE11 versus ([^{64}Cu]Cu-NOTA)$_3$-C225 using vital A431 cells at 4 °C (white triangles) and 37 °C (black triangles). The curves illustrate data of one representative assay. Data points are the mean of three samples ± SD

In a second competition study, EGF should displace GE11 (without modification). On serum-starved A431 cells, EGF induced the phosphorylation of the EGFR at Y1173-position (tyr), one of the three major phosphorylation sites at the regulatory domain (Fan et al. 2005); this phosphorylation could in turn be reduced by C225 (Fig. 8). No change in the phosphorylation state could be observed by treating A431 cells with GE11 or C225 alone. However, it was intended to show whether GE11 could either block or stimulate the activation of pEGFR, GE11 could not inhibit the phosphorylation, even not at 10000-fold excess over EGF.

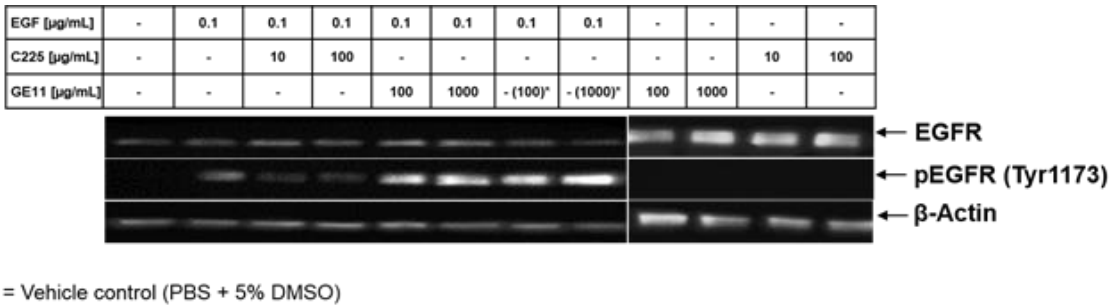

* = Vehicle control (PBS + 5% DMSO)

Fig. 8 Immunologic detection of EGFR (Y1173) phosphorylation levels, EGFR and β-actin upon treatment with EGF in combination with C225 or GE11. Vehicle control was PBS + 5% DMSO. Western blot analysis (lower part) was performed for phosphorylated EGFR (pEGFR, Y1173), total EGFR, and β-actin by incubation with respective primary antibodies followed by incubation with HRP-coupled secondary antibodies and chemiluminescence detection. The different intensity of β-actin and EGFR bands occurred since the blot of the last 4 lanes on the right side was obtained from a separated immunoblotting assay. The data represent only qualitative estimation. Similar results were obtained in three independent experiments

In contrast to C225, the phosphorylation degree seems to be increased when EGF and GE11 were added in combination to A431 cells. However, this increase also appeared for the GE11 vehicle control (PBS + 5% DMSO).

In vivo studies

Biodistribution studies of the radiolabeled peptides [^{64}Cu]Cu-**1** and [^{64}Cu]Cu-**2** were carried out in healthy rats; the organs were measured 5 and 60 min after injection of the tracer. Notably uptake was determined only in the excretory organs; in the other organs investigated, the SUVs were lower or about 1 (Fig. S2, Table S1). Fig. 9 shows levels of total uptake in kidney, liver, intestine, stomach and urine. The uptake of [^{64}Cu]Cu-**2** was higher than of [^{64}Cu]Cu-**1** in intestine, and in liver only 5 min p.i. The levels of both radioconjugates decreased slightly in kidney 60 min after injection. The [^{64}Cu]Cu-

1 and [^{64}Cu]Cu-**2** levels in the liver was low after 60 min. In intestine and urine, the uptake of both radioconjugates increased strong 60 min p.i. (Fig. 9).

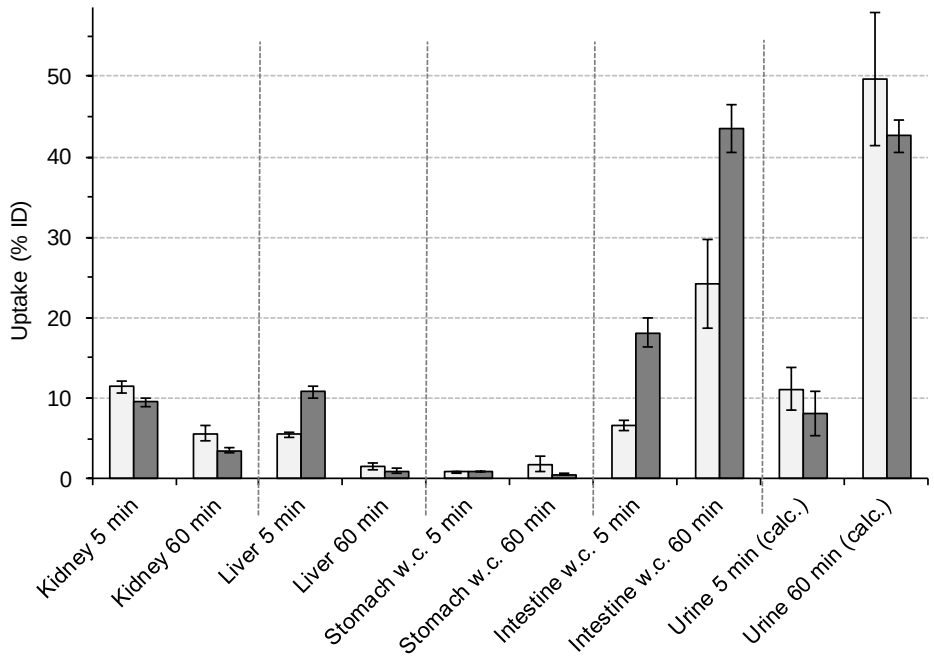

Fig. 9 Biodistribution of [^{64}Cu]Cu-**1** (white columns), [^{64}Cu]Cu-**2** (gray columns) in the excretory organs of healthy rats in % ID (n = 8), 5 min and 60 min p.i.; *intestine and urine data are presented in % ID

The blood clearance was investigated and showed an elimination half-life of 3 min for [^{64}Cu]Cu-**1** and 3.3 min for [^{64}Cu]Cu-**2** (Fig. 10). The stability of [^{64}Cu]Cu-**1** and [^{64}Cu]Cu-**2** determined from in vivo blood samples (Fig. S1) resulted in only around 60% of both original tracers, 3 min p.i. After 10 min only about 10% of both conjugates was left (Fig. 11).

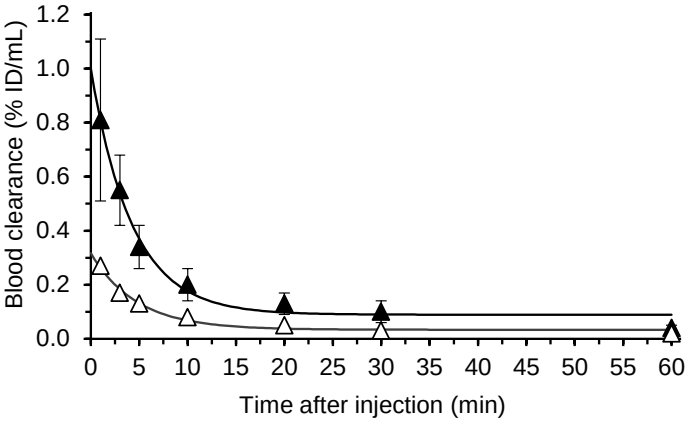

Fig. 10 Blood clearance of [^{64}Cu]Cu-**1** (black triangles) and [^{64}Cu]Cu-**2** (empty triangles) from venous blood of Wistar rats, (uncorrected for metabolite formation)

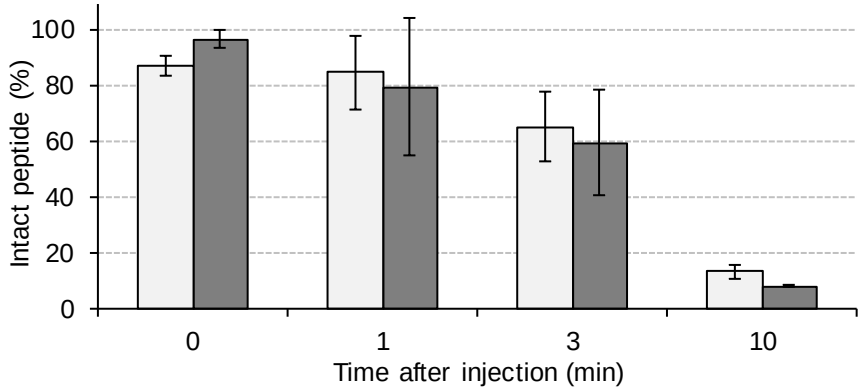

Fig. 11 Stability of [^{64}Cu]Cu-**1** (white columns) and [^{64}Cu]Cu-**2** (gray columns) in blood plasma of healthy rats.

PET images (Fig. 12A,B) showed a high uptake of [^{64}Cu]Cu-**1** and [^{64}Cu]Cu-**2** in kidney and bladder 5 min p.i. Towards image acquisition times of 20 min or 60 min the uptake in the intestines increased. Concerning the uptake in the tumor,

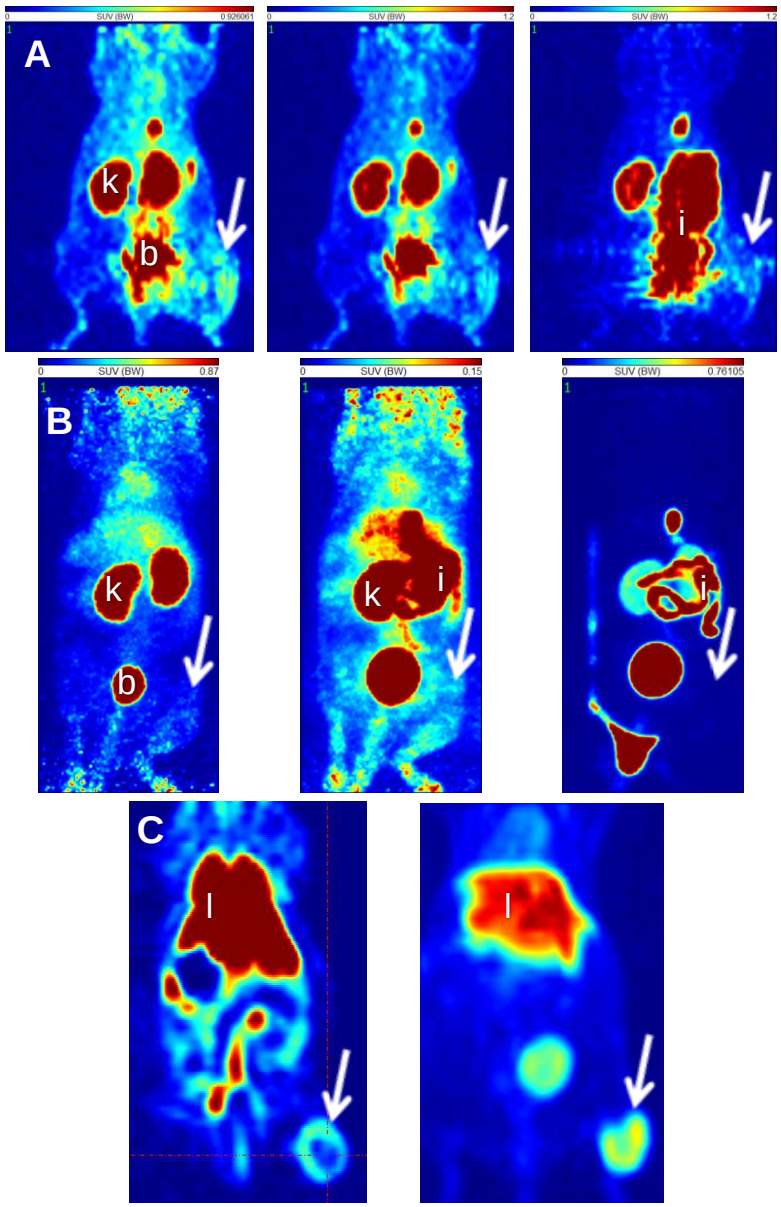

Fig. 12 PET images of (**A**) [^{64}Cu]Cu-**1** and (**B**) [^{64}Cu]Cu-**2** from FaDu tumor bearing mice, 5 min (left), 20 min (middle) and 60 min (right) p.i.; (**C**) PET images of ([^{64}Cu]Cu-NOTA)$_3$-C225 from FaDu tumor bearing mice, 2 h (left) and 23 h (right) p.i.; the arrows indicate the position of EGFR-FaDu-tumor; b: bladder, i: intestine, k: kidney, l: liver

some accumulation of [^{64}Cu]Cu-**1** could be observed 5 min p.i., thereafter the activity decreased (Fig. 12A). For [^{64}Cu]Cu-**2**, a rather blurred low tumor accumulation was observed (Fig. 12B) 5 and 20 min p.i. In comparison, PET images after ([^{64}Cu]Cu-NOTA$_3$)-C225 injection revealed clear tumor uptake 2 h p.i. that increased 23 h i.p., however a high liver uptake can be observed. The PET images from [^{64}Cu]Cu-**1**, [^{64}Cu]Cu-**2** and ([^{64}Cu]Cu-NOTA$_3$)-C225 were not standardized to each other as the principle purpose was to visualize the tumor site only qualitatively.

The low appearance of radioactive substance in the tumor of the two labeled conjugates can be compared by SUVs directly, confirming a lower tumor accumulation with [^{64}Cu]Cu-**2** for the complete PET recording (Fig. 13A). For the two labeled peptides the tumor-to-muscle ratio increased for [^{64}Cu]Cu-**1** until about 60 min and for [^{64}Cu]Cu-**2** until about 45 min (Fig. 13B).

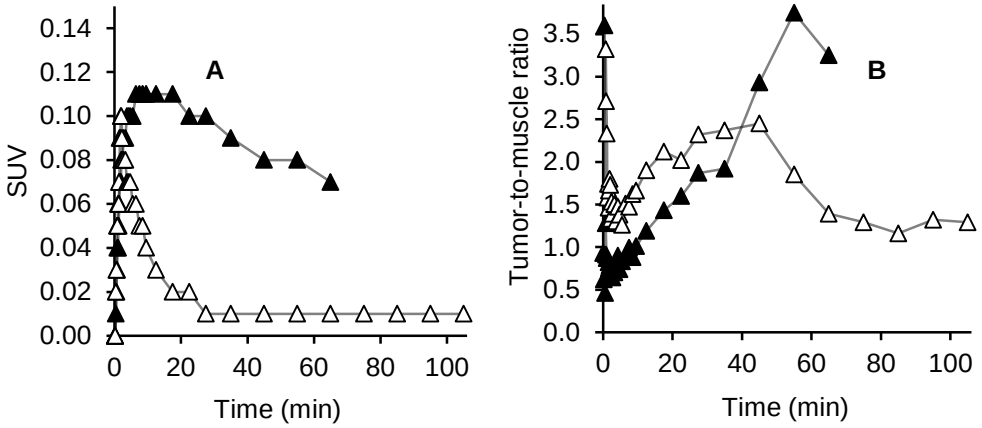

Fig. 13 (**A**) SUVs and (**B**) tumor-to-muscle ratios of [^{64}Cu]Cu-**1** (black triangles) and [^{64}Cu]Cu-**2** (empty triangles)

The highest tumor-to-muscle ratio was determined for [^{64}Cu]Cu-**1** with a value of 3.75 at 60 min p.i. The highest values for [^{64}Cu]Cu-**2** was about 2.5 after 45 min (Fig. 13B). Even if the appearance of [^{64}Cu]Cu-**2** in the tumor was low, the tumor-to-muscle ratios were slightly higher until 40 min p.i. compared to [^{64}Cu]Cu-**1**.

Discussion

Since the EGFR is overexpressed in a wide range of epithelial carcinoma it has long been pursued for molecular cancer therapy, whereby monoclonal antibodies such as C225 have been successfully applied (Sihver et al. 2014). However, for PET imaging, a major drawback of monoclonal antibodies is their large size resulting in slow tumor accumulation and undesired enrichment in the liver. Hence, smaller radioligands, such as targeted peptides, possess several attractive characteristics (Signore et al. 2001; Reubi and Maecke 2008). The dodecapeptide GE11 was reported to bind specifically at the EGFR and furthermore exhibited promising results when conjugated with large chemical groups (Li et al. 2005). Thus, it is reasonable to assume that conjugating β-Ala-GE11 with an EG-based linker and ^{64}Cu-NOTA will hardly affect the radiopharmacological properties. Nonetheless, the pharmacological characteristics, regarding binding affinity, selectivity, metabolism and biological activity had to be validated in vitro using EGFR-rich and EGFR-poor cell preparations. Furthermore, preliminary in vivo studies should show a trend as to whether one of the radioconjugates might be appropriate for future applications.

Peptides

β-Ala-GE11 and β-Ala-GE11-NH_2 were conjugated successfully and in sufficient yields with the EG-based linker and the chelator *p*-SCN-Bn-NOTA. The bifunctional linker has also been linked directly to the N-terminal amino group of β-Ala in β-Ala-GE11 but has not been further characterized biologically since it was hardly water soluble.

The radiolabeled conjugates showed very weak shoulders in the HPLC results that could be justified by the phenomenon of an isomer formation after complexation with ^{64}Cu after labeling (Schlesinger et al. 2011). Furthermore, they showed high stability in buffer and cell medium and in human serum for at least 2 h. It is known that C-terminal amides might prevent degradation by endopeptidases (Brinckerhoff et al. 1999; Landon et al. 2004), thereby increasing the in vivo stability; thus, after 24 h the serum stability of the amid conjugate [^{64}Cu]Cu-**2** was found to be higher (70%) than for [^{64}Cu]Cu-**1** (50%). Since the aim was tumor imaging as a diagnostic method high peptide stability is required. The analysis of [^{64}Cu]Cu-**1** in MALDI-TOF resulted, presumably in two main metabolites and the original compound, whereby the cleavage was assumed to be within the peptide. The induction of the fragmentation was assumed to be caused primarily by peptidases in the serum (Stewart and Gilvarg 1999; Moughan and Stevens 2013).

In vitro characterization

The cell viability tests with the β-Ala-GE11 peptide, up to a concentration of 130 µM (210 µg/ml β-Ala-GE11) revealed no change in viability using the applied cancer cells, whereas Li *et al.* (2005) showed stimulated growth of around 10% for EGFR expressing human hepatoma cells after GE11 treatment (1 µg/mL). Their data suggest that GE11 acts as partial EGFR agonist, since human EGF also stimulated the growth by about 50%. In another study, treatment with phthalocyanine-GE11 conjugates on A431 (and other cell lines) showed somewhat decreased cell viability after 24 h, however with a fluorescence-based assay (cell titer blue) (Ongarora et al. 2012). Furthermore, PEG-liposome-GE11 conjugates did not exhibit any change in cell viability after 48 h on EGFR expressing lung carcinoma cells (Cheng et al.2014). Obviously from these studies, conjugates of GE11 show no or only minor influence concerning cell viability. Further evidence that GE11 does not exert physiological effects could be proved with the attempted immunologic detection of EGFR (Y1173) phosphorylation upon treatment with GE11 (up to 1 mg/mL). It neither stimulated EGFR phosphorylation nor decreased the phosphorylation degree after pre-stimulation with EGF. The enhanced phosphorylation level in the Western blot, after GE11 addition (Fig. 8, lane 5 to 8) might appear due to the vehicle DMSO (Rubin and Earp 1983; Luetteke et al. 1994).

Saturation binding assays with ([^{64}Cu]Cu-$NOTA_3$)-C225 resulted in high specific binding and good affinities at A431 and FaDu cells, whereas no binding was observed using the non-EGFR expressing MDA-MB-435s cells. For C225 high affinities have been previously reported (0.1-0.2 nM) (Goldstein et al. 1995). The affinity of the radiolabeled antibody with K_d-values in the low nanomolar range, is definitely sufficiently high. With regard to the determined B_{max}-values, it was verified that A431 cells have a several fold higher EGFR density then FaDu cells. On living cells, the affinity is temperature-dependent, thus internalization processes should be considered (Fan et al. 1994; Prewett et al. 1996). Such processes are usually inhibited at 4 °C and will not appear in cell homogenates.

Saturation assays with [^{64}Cu]Cu-**1** and potentially stabilized [^{64}Cu]Cu-**2**, resulted in linear binding isotherms, i.e. not hyperbolic. The level of total and nonspecific binding was similarly high, and no bound part could be measured, neither on intact cells nor in homogenate, at either incubation temperatures, and w/ or w/o protein serum. These data show that the radioconjugates were not able to target the EGFR under in vitro conditions. Thus, the outcome of the binding studies with [^{64}Cu]Cu-**1** and [^{64}Cu]Cu-**2** differs strongly from the results of Li et al. (2005) and Song *et al*. (2008) who reported to have observed a high EGFR affinity and specificity of GE11-based conjugates. These contradictory results might

suggest that conjugation with the linker and bifunctional chelator (BFC) *p*-SCN-Bn-NOTA, alters the chemical characteristics of the GE11-peptide (*e.g.* charge, size and polarity) leading to a loss in EGFR affinity and specificity. Therefore, the binding ability of GE11 alone was determined. Since EGF and GE11 share the same EGFR binding site as reported by Ongarora *et al*. (2012) GE11 should have the potency to compete with bound EGF from the receptor. Indeed, effective GE11-blocking was shown with EGF also being able to displace GE11 from the EGFR (Li et al. 2005). Aditionally, C225 can block EGF-binding and EGF-induced EGFR autophosphorylation (Fan et al. 1994; Ferraro et al. 2013). Though, the EGFR-targeting ability of GE11 was determined by displacement assays with ([^{64}Cu]Cu-NOTA$_3$)-C225. Once more, GE11 was not able to block or displace the binding ligand from the EGFR. In conclusion, the inability of [^{64}Cu]Cu-**1** and [^{64}Cu]Cu-**2** to bind at the receptor is not due to chemical alterations by adding of linker and BFC, but rather a general incapability of GE11 alone.

Interestingly, some studies also show a poor to negligible targeting-ability of GE11. For example, Abourbeh *et al.* (2012) quantified the binding parameter of [^{124}I]I-GE11 and [^{125}I]I-EGF on A431 cells. Whereas [^{125}I]I-EGF exposed a similar binding affinity as described in literature (K_d ~ low nanomolar range) (Björkelund et al. 2011) [^{124}I]-GE11 showed high nonspecific binding (80-90%). In an [^{125}I]-EGF displacement assay, GE11 (up to 1 mM) was not able to dislocate EGF from the EGFR. But when GE11 was tethered with PEG-PEI the binding affinity to the EGFR was increased and with polyinosine/cytosine complexation the targeting-potency was enhanced (Abourbeh et al. 2012). Ongarora *et al*. (2012) synthesized phthalocyanine-GE11 conjugates for potential use in photodynamic therapy of colorectal cancer. Using docking studies, they were able to modulate the GE11-EGFR interactions and derived two important results: (I) GE11 interacts over hydrogen-bonding interactions of the amino acids residues Y2 and I13 with the EGF-binding pocket. (II) The peptide did not offer an overall secondary structure. The docking energy of the phthalocyanine-GE11 conjugates was lower than for GE11 alone due to additional interactions of phthalocyanine with the EGFR. Thus, binding affinities could be confirmed by surface plasmon resonance measurements. However, despite the promising results it was not possible to detect binding of the conjugates on living cells (e.g. A431). This, together with the high hydrophobic character of GE11, led to the suggestion that the peptide has a strong tendency for aggregation preventing the EGFR-targeting ability (Ongarora et al. 2012). Results from a study with a Cy-dye and PEG based linked GE11 represented a measurable but low affinity (μM range), in glioblastoma cells (Agnes et al. 2012). A recent study with ^{99m}Tc labeled HYNIC-GE11 revealed an affinity of 73 nM in ovarian tumor cells (Rahmanian et al. 2017). Presumably, they measured the cell uptake favored by the linkers. When comparing studies with synthesized GE11-based conjugates, it becomes evident that the conjugates that successfully targeted the EGFR were tethered to PEI or PEG (Li et al. 2005; Klutz et al. 2011a, b; Abourbeh et al. 2012; Mickler et al. 2012), or to cationic dendrimers (Grünwald et al. 2013). All of these components are highly hydrophilic suggesting aggregate formation.

In vivo experiments

Since, in recent studies, the affinity and specificity of ^{125}I-labeled GE11 has been described (Li et al. 2005), even if in the present study these properties could not be confirmed, but a good in vitro stability could be measured, a pilot small animal study should provide conclusive radiopharmacological information. Notably, the in vivo experiments were performed in parallel to the in vitro studies once the conjugates were labeled successfully. The amide group at the C-terminus of [^{64}Cu]Cu-**2** was introduced to stabilize the peptide against proteolytic degradation and for slower clearance. Such arrangement implicated higher uptake in liver and intestine. However, other biodistribution studies have been done in mice bearing EGFR expressing tumor xenografts. For example, in the study of Li et al. (2005) a tumor uptake of 6 %ID/g for ^{125}I-labeled GE11 at 30 min p.i. and still more than 3 %ID/g at 4 h p.i. was presented but they did not demonstrate the

peptide stability in blood and formation of metabolites (Li et al. 2005). In recent studies, the majority of GE11-peptide constructs investigated were tethered to other large molecules. This seems to be a reason for the slower uptake and clearance in body and tumor. Tethered peptides exhibited a higher uptake in the liver than in the kidney (Klutz et al. 2011a; Lee et al. 2015), whereby tumor accumulation was also higher than in the liver in the study of Klutz et al. (2011a). Likewise, some tumor uptake has been demonstrated after administration of EGFR targeted thiolated gelatin nanoparticles, however, the accumulation was very high in the liver, spleen and kidney (Xu et al. 2013). In vivo experiments with ^{99m}Tc-HYNIC-GE11 also showed low tumor uptake and similar tumor-to-muscle ratios as those of present study, but really high values in the kidney (Rahmanian et al. 2017). A GE11-liposome conjugate showed high uptake in liver and spleen up to 24 h p.i., however, some tumor accumulation has been detected after 12h p.i (Cheng et al. 2014). One phenomenon responsible for tumor uptake of large molecules, and perhaps large GE11 conjugate constructs is the enhanced permeability and retention (EPR) effect. Due to aberrant formations of tumor blood vessels and malfunctions of lymphatic vessels in tumor tissue the clearance of macromolecules and lipids is impaired, so that they remain in the tumor for a longer time (Fang et al. 2011). The non-tethered peptides in the present study showed low tumor uptake. Since the tracer molecules were rather small an EPR effect might be barely noticeable.

Summary and Conclusions

The β-Ala-GE11 peptide and its stabilized version β-Ala-GE11-NH_2, were successfully conjugated to an EG-based linker and with the BFC *p*-SCN-Bn-NOTA for further labeling with ^{64}Cu. The labeled conjugates were stable in buffer or cell medium. However, degradation in human serum after 24 h could be delayed to some extend by amidation of the free C-terminus. The binding affinity of the radiolabeled GE11-conjugates to EGFR failed to be determined in saturation and competition studies with cell lines of high EGFR expression. Biodistribution in rats as well as PET images from EGFR expressing tumor bearing mice showed notably accumulation of the labeled conjugates in the excretion organs. Whereas the uptake in the tumor itself was comparatively low, with a maximal tumor to muscle ratio of 3.75 for [^{64}Cu]Cu-**1**, 1 h p.i. Since for these types of small conjugates a strong tendency for aggregation is suggested, they do not represent suitable leads for novel EGFR-targeted imaging probes. Moreover, the rapid metabolism presumably also due to the linear nature of the peptides implies the need of peptide modification for stability improvement and/or better bioavailability for suitability as in vivo imaging and/or therapeutic agents. Efforts should focus on derivatives tethered with liposomes, PEGs and/or PEI, or, more promisingly, on other, e.g., antibody-based approaches.

Compliance with ethical standards

Ethical approval The animal experiments were performed in accordance to the guidelines of the German Regulations of Animal Welfare. The protocol was approved by the local Ethical Committee for Animal Experiments (reference number 24-9168.21-4/2004-1).

Conflict of interest The authors have no conflict of interest to declare.

References

Abourbeh G, Shir A, Mishani E, Ogris M, Rödl W, Wagner E, Levitzki A (2012) PolyIC GE11 polyplex inhibits EGFR-overexpressing tumors. IUBMB Life 64: 324-330. doi: 10.1002/iub.1002

Agnes RS, Broome AM, Wang J, Verma A, Lavik K, Basilion JP (2012) An optical probe for noninvasive molecular imaging of orthotopic brain tumors overexpressing epidermal growth factor receptor. Mol Cancer Ther 11: 2202-2211. doi: 10.1158/1535-7163.MCT-12-0211

Ang KK, Berkey BA, Tu X, Zhang HZ, Katz R, Hammond EH, Fu KK, Milas L (2002) Impact of epidermal growth factor receptor expression on survival and pattern of relapse in patients with advanced head and neck carcinoma. Cancer Res 62: 7350-7356

Banerjee SS, Aher N, Patil R, Khandare J (2012) Poly(ethylene glycol)-Prodrug Conjugates: Concept, Design, and Applications. J Drug Deliv 2012:103973. doi: 10.1155/2012/103973

Baumann M, Krause M (2004) Targeting the epidermal growth factor receptor in radiotherapy: radiobiological mechanisms, preclinical and clinical results. Radiother Oncol 72: 257-266. doi: 10.1016/j.radonc.2004.07.007

Bergmann R, Ruffani A, Graham B, Spiccia L, Steinbach J, Pietzsch J, Stephan H (2013) Synthesis and radiopharmacological evaluation of ^{64}Cu-labeled bombesin analogs featuring a bis(2-pyridylmethyl)-1,4,7-triazacyclononane chelator. Eur J Med Chem 70: 434-446. doi: 10.1016/j.ejmech.2013.10.013

Björkelund H, Gedda L, Andersson K (2011) Comparing the epidermal growth factor interaction with four different cell lines: intriguing effects imply strong dependency of cellular context. PLoS One 6: e16536. doi: 10.1371/journal.pone.0016536

Brinckerhoff LH, Kalashnikov VV, Thompson LW, Yamshchikov GV, Pierce RA, Galavotti HS, Engelhard VH, Slingluff CL Jr (1999) Terminal modifications inhibit proteolytic degradation of an immunogenic MART-1(27-35) peptide: implications for peptide vaccines. Int J Cancer 83: 326-334

Bröer S (2008) Amino acid transport across mammalian intestinal and renal epithelia. Physiol Rev 88: 249-286. doi: 10.1152/physrev.00018.2006

Chanda N, Zambre A, Shukla R, Mukharjee P, Mukhopadhyay D, Boote E, Kannan R, Katti KV (2010) Relative study between anti-EGFR and GE11 peptide conjugated gold nanoparticles for in vivo targeting in pancreatic cancer. https://mospace.umsystem.edu/xmlui/handle/10355/9779. Accessed 26 Octobre 2017

Chen K, Chen X (2010) Design and development of molecular imaging probes. Curr Top Med Chem 10:1227-1236

Cheng L, Huang FZ, Cheng LF, Zhu YQ, Hu Q, Li L, Wei L, Chen DW (2014) GE11-modified liposomes for non-small cell lung cancer targeting: preparation, ex vitro and in vivo evaluation. Int J Nanomedicine 9: 921-935. doi: 10.2147/IJN.S53310

DeJesus OT (2012) Synthesis of [64Cu]Cu-NOTA-Bn-GE11 for PET imaging of EGFR-rich tumors. Curr Radiopharm 5: 15-18

Di L (2015) Strategic approaches to optimizing peptide ADME properties. AAPS J 17: 134-143. doi: 10.1208/s12248-014-9687-3

van Dijk LK, Boerman OC, Kaanders JH, Bussink J (2015) PET Imaging in Head and Neck Cancer Patients to Monitor Treatment Response: A Future Role for EGFR-Targeted Imaging. Clin Cancer Res 21: 3602-3609. doi: 10.1158/1078-0432.CCR-15-0348

Dissoki S, Hagooly A, Elmachily S, Mishani E (2011) Labeling approaches for the GE11 peptide, an epidermal growth factor receptor biomarker. J Labelled Compd Rad 54: 693-701. doi: 10.1002/jlcr.1910

Fan YX, Wong L, Johnson GR (2005) EGFR kinase possesses a broad specificity for ErbB phosphorylation sites, and ligand increases catalytic-centre activity without affecting substrate binding affinity. Biochem J 392: 417-423. doi: 10.1042/BJ20051122

Fan Z, Lu Y, Wu X, Mendelsohn J (1994) Antibody-induced epidermal growth factor receptor dimerization mediates inhibition of autocrine proliferation of A431 squamous carcinoma cells. J Biol Chem 269: 27595-27602

Fang J, Nakamura H, Maeda H (2011) The EPR effect: Unique features of tumor blood vessels for drug delivery, factors involved, and limitations and augmentation of the effect. Adv Drug Deliv Rev 63: 136-151. doi: 10.1016/j.addr.2010.04.009

Ferraro DA, Gaborit N, Maron R, Cohen-Dvashi H, Porat Z, Pareja F, Lavi S, Lindzen M, Ben-Chetrit N, Sela M, Yarden Y (2013) Inhibition of triple-negative breast cancer models by combinations of antibodies to EGFR. Proc Natl Acad Sci U S A 110: 1815-1820. doi: 10.1073/pnas.1220763110

Genta I, Chiesa E, Colzani B, Modena T, Conti B, Dorati R (2018) GE11 Peptide as an Active Targeting Agent in Antitumor Therapy: A Minireview. Pharmaceutics 10, pii: E2. doi: 10.3390/pharmaceutics10010002

Goldstein NI, Prewett M, Zuklys K, Rockwell P, Mendelsohn J (1995) Biological efficacy of a chimeric antibody to the epidermal growth factor receptor in a human tumor xenograft model. Clin Cancer Res 1: 1311-1318.

Grünwald GK, Vetter A, Klutz K, Willhauck MJ, Schwenk N, Senekowitsch-Schmidtke R, Schwaiger M, Zach C, Wagner E, Göke B, Holm PS, Ogris M, Spitzweg C (2013) EGFR-Targeted Adenovirus Dendrimer Coating for Improved Systemic Delivery of the Theranostic NIS Gene. Mol Ther Nucleic Acids 2: e131. doi: 10.1038/mtna.2013.58.

Gutiérrez-García VM, Reyes-Rangel G, Muñoz-Muñiz O, Juaristi E (2001) Enantioselective synthesis of β-amino acids. 12. Experimental and theoretical study of the diastereoselectivity of alkylation of the dianion of N',N'-bis(α-phenylethyl)-N-carbobenzyloxypropionamide. J Braz Chem Soc 12: 652-660

Haigler H, Ash JF, Singer SJ, Cohen S (1978) Visualization by fluorescence of the binding and internalization of epidermal growth factor in human carcinoma cells A-431. Proc Natl Acad Sci U S A 75: 3317-3321

Heldt JM, Kerzendörfer O, Mamat C, Starke F, Pietzsch HJ, Steinbach J (2013) Synthesis of short and versatile heterobifunctional linkers for conjugation of bioactive molecules with (radio-)labels. Synlett 24: 432-436. doi: 10.1055/s-0032-1318198

Hofman MS, Kong G, Neels OC, Eu P, Hong E, Hicks RJ (2012) High management impact of Ga-68 DOTATATE (GaTate) PET/CT for imaging neuroendocrine and other somatostatin expressing tumours. J Med Imaging Radiat Oncol 56: 40-47. doi: 10.1111/j.1754-9485.2011.02327.x

Klutz K, Schaffert D, Willhauck MJ, Grünwald GK, Haase R, Wunderlich N, Zach C, Gildehaus FJ, Senekowitsch-Schmidtke R, Göke B, Wagner E, Ogris M, Spitzweg C (2011a) Epidermal growth factor receptor-targeted (131)I-therapy of liver cancer following systemic delivery of the sodium iodide symporter gene. Mol Ther 19: 676-685. doi: 10.1038/mt.2010.296

Klutz K, Willhauck MJ, Dohmen C, Wunderlich N, Knoop K, Zach C, Senekowitsch-Schmidtke R, Gildehaus FJ, Ziegler S, Fürst S, Göke B, Wagner E, Ogris M, Spitzweg C (2011b) Image-guided tumor-selective radioiodine therapy of liver cancer after systemic nonviral delivery of the sodium iodide symporter gene. Hum Gene Ther 22:1563-1574. doi: 10.1089/hum.2011.041

Koi L, Bergmann R, Bruchner K, Pietzsch J, Pietzsch HJ, Krause M, Steinbach J, Zips D, Baumann M (2014) Radiolabeled anti-EGFR-antibody improves local tumor control after external beam radiotherapy and offers theragnostic potential. Radiother Oncol 110: 362-369. doi: 10.1016/j.radonc.2013.12.001

Kondo M, Kimura M, Sato K, Horimoto H (1987) Synthesis and properties of [1,1'-bis(α-aminoisobutyric acid)]gramicidin S and [1- α-aminoisonutyric acid]semigramicidin S. Bull Chem Soc Jpn 60: 1391-1397

Landon LA, Zou J, Deutscher SL (2004) Is phage display technology on target for developing peptide-based cancer drugs? Curr Drug Discov Technol 1: 113-132

Lee D, Lee YM, Kim J, Lee MK, Kim WJ (2015) Enhanced tumor-targeted gene delivery by bioreducible polyethylenimine tethering EGFR divalent ligands. Biomater Sci 3: 1096-1104. doi: 10.1039/c5bm00004a

Li Z, Zhao R, Wu X, Sun Y, Yao M, Li J, Xu Y, Gu J (2005) Identification and characterization of a novel peptide ligand of epidermal growth factor receptor for targeted delivery of therapeutics. FASEB J 19: 1978-1985. doi: 10.1096/fj.05-4058com

Lindenberg L, Adler S, Turkbey IB, Mertan F, Ton A, Do K, Kummar S, Gonzalez EM, Bhattacharyya S, Jacobs PM, Choyke P (2017) Dosimetry and first human experience with 89Zr-panitumumab. Am J Nucl Med Mol Imaging 7: 195-203

van Loon J, Even AJG, Aerts HJWL, Öllers M, Hoebers F, van Elmpt W, Dubois L, Dingemans AC, Lalisang RI, Kempers P, Brans B, Winnepenninckx V, Speel EJ, Thunnissen E, Smits KM, Boellaard R, Vugts DJ, De Ruysscher D, Lambin P (2017) PET imaging of zirconium-89 labelled cetuximab: A phase I trial in patients with head and neck and lung cancer. Radiother Oncol 122: 267-273. doi: 10.1016/j.radonc.2016.11.020

Luetteke NC, Phillips HK, Qiu TH, Copeland NG, Earp HS, Jenkins NA, Lee DC (1994) The mouse waved-2 phenotype results from a point mutation in the EGF receptor tyrosine kinase. Genes Dev 8: 399-413

Martinez-Useros J, Garcia-Foncillas (2015) The challenge of blocking a wider family members of EGFR against head and neck squamous cell carcinomas. Oral Oncol 51: 423-430. doi: 10.1016/j.oraloncology.2015.02.092

Master A, Malamas A, Solanki R, Clausen DM, Eiseman JL, Sen Gupta A (2013) A cell-targeted photodynamic nanomedicine strategy for head and neck cancers. Mol Pharm 10: 1988-1997. doi: 10.1021/mp400007k

Mendelsohn J, Baselga J (2006) Epidermal growth factor receptor targeting in cancer. Semin Oncol 33: 369-385. doi: 10.1053/j.seminoncol.2006.04.003

Mickler FM, Möckl L, Ruthardt N, Ogris M, Wagner E, Bräuchle (2012) Tuning nanoparticle uptake: live-cell imaging reveals two distinct endocytosis mechanisms mediated by natural and artificial EGFR targeting ligand. C. *Nano Lett* 12: 3417-23

Moughan PJ, Stevens BR (2013) Chapter 9; Digestion and absorption of protein. In: Stipanuk MH, Caudill MA (ed) Biochemical, physiological, and molecular aspectsof human nutrition, 3rd edn. Elsevier Saunders, St. Louis, pp 162-178

Nicholson RI, Gee JM, Harper ME (2001) EGFR and cancer prognosis. Eur J Cancer 37: 9-15

Ongarora BG, Fontenot KR, Hu X, Sehgal I, Satyanarayana-Jois SD, Vicente MG (2012) Phthalocyanine-peptide conjugates for epidermal growth factor receptor targeting. J Med Chem 55: 3725-3738. doi: 10.1021/jm201544y

Petrulli JR, Hansen SB, Abourbeh G, Yaqub M, Bahce I, Holden D, Huang Y, Nabulsi NB, Contessa JN, Mishani E, Lammertsma AA, Morris ED (2017) A multi species evaluation of the radiation dosimetry of [11C]erlotinib, the radiolabeled analog of a clinically utilized tyrosine kinase inhibitor. Nucl Med Biol 47: 56-61. doi: 10.1016/j.nucmedbio.2016.12.009

Prewett M, Rockwell P, Rockwell RF, Mendelsohn J, Scher HI, Goldstein NI (1996) The biologic effects of C225, a chimeric monoclonal antibody to the EGFR, on human prostate carcinoma. J Immunother Emphasis Tumor Immunol 19: 419-427

Rahmanian N, Hosseinimehr SJ, Khalaj A, Noaparast Z, Abedi SM, Sabzevari O (2017) 99mTc-radiolabeled GE11-modified peptide for ovarian tumor targeting. Daru 25: 13. doi: 10.1186/s40199-017-0179-8

Ren H, Gao C, Zhou L, Liu M, Xie C, Lu W (2015) EGFR-targeted poly(ethylene glycol)-distearoylphosphatidyl ethanolamine micelle loaded with paclitaxel for laryngeal cancer: preparation, characterization and in vitro evaluation. Drug Deliv 22, 785-794. doi: 10.3109/10717544.2014.896057

Reubi JC, Maecke HR (2008) Peptide-based probes for cancer imaging. J Nucl Med 49: 1735-1738. doi: 10.2967/jnumed.108.053041

Rubin RA, Earp HS (1983) Dimethyl sulfoxide stimulates tyrosine residue phosphorylation of rat liver epidermal growth factor receptor. Science 219: 60-63

Salomon DS, Brandt R, Ciardiello F, Normanno N (1995) Epidermal growth factor-related peptides and their receptors in human malignancies. Crit Rev Oncol Hematol 19: 183-232

Schlesinger J, Rajander J, Ihalainen JA, Ramesh D, Eklund P, Fagerholm V, Nuutila P, Solin O (2011) Isomerism of [64Cu-NOTA-Bn]-labeled radiotracers: separation of two complex isomers and determination of their interconversion energy barrier using ion pair chromatography. Inorg Chem 50: 4260-4271. doi: 10.1021/ic101775q

Schubert M, Bergmann R, Förster C, Sihver, W, Vonhoff S, Klussmann S, Bethge L, Walther M, Schlesinger J, Pietzsch J, Steinbach J, Pietzsch HJ (2017) Novel tumor pretargeting system based on complementary l-configured oligonucleotides. Bioconjug Chem 28: 1176-1188. doi: 10.1021/acs.bioconjchem.7b00045

Schütze C, Dörfler A, Eicheler W, Zips D, Hering S, Solca F, Baumann M, Krause M (2007) Combination of EGFR/HER2 tyrosine kinase inhibition by BIBW 2992 and BIBW 2669 with irradiation in FaDu human squamous cell carcinoma. Strahlenther Onkol 183: 256-264. doi: 10.1007/s00066-007-1696-z

Selvaggi G, Novello S, Torri V, Leonardo E, De Giuli P, Borasio P, Mossetti C, Ardissone F, Lausi P, Scagliotti GV (2004) Epidermal growth factor receptor overexpression correlates with a poor prognosis in completely resected non-small-cell lung cancer. Ann Oncol 15: 28-32

Signore A, Annovazzi A, Chianelli M, Corsetti F, Van de Wiele C, Watherhouse RN (2001) Peptide radiopharmaceuticals for diagnosis and therapy. Eur J Nucl Med 28: 1555-1565. doi: 10.1007/s002590100583

Sihver W, Pietzsch J, Krause M, Baumann M, Steinbach J, Pietzsch HJ (2014) Radiolabeled Cetuximab Conjugates for EGFR Targeted Cancer Diagnostics and Therapy. Pharmaceuticals (Basel) 7: 311-338. doi: 10.3390/ph7030311

Song S, Liu D, Peng J, Sun Y, Li Z, Gu JR, Xu Y (2008) Peptide ligand-mediated liposome distribution and targeting to EGFR expressing tumor in vivo. Int J Pharm 363: 155-161. doi: 10.1016/j.ijpharm.2008.07.012

Stewart JD, Gilvarg C (1999) Determination of the activity of carboxypeptidase A in the blood of healthy human adults. Clin Chim Acta 281: 19-28

Tang H, Chen X, Rui M, Sun W, Chen J, Peng J, Xu Y (2014) Effects of surface displayed targeting ligand GE11 on liposome distribution and extravasation in tumor. Mol Pharm 11: 3242-3250. doi: 10.1021/mp5001718

Thieme S, Walther M, Pietzsch HJ, Henniger J, Preusche S, Mäding P, Steinbach J (2012) Module-assisted preparation of 64Cu with high specific activity. Appl Radiat Isot 70: 602-608. doi: 10.1016/j.apradiso.2012.01.019

Tsutsui S, Kataoka A, Ohno S, Murakami S, Kinoshita J, Hachitanda Y (2002) Prognostic and predictive value of epidermal growth factor receptor in recurrent breast cancer. Clin Cancer Res 8: 3454-3460

Wee P, Wang Z (2017) Epidermal growth factor receptor cell proliferation signaling pathways. Cancers 9: pii:E52. doi: 10.3390/cancers9050052

Xu J, Gattacceca F, Amiji M (2013) Biodistribution and pharmacokinetics of EGFR-targeted thiolated gelatin nanoparticles following systemic administration in pancreatic tumor-bearing mice Mol Pharm 10: 2031-2044. doi: 10.1021/mp400054e

Yoshimoto M, Kurihara H2, Fujii H (2015) Theragnostic imaging using radiolabeled antibodies and tyrosine kinase inhibitors. ScientificWorldJournal 2015: 842101. doi: 10.1155/2015/842101

Yu HM, Chen JH, Lin KL, Lin WJ (2015) Synthesis of (68)Ga-labeled NOTA-RGD-GE11 heterodimeric peptide for dual integrin and epidermal growth factor receptor-targeted tumor imaging. J Labelled Compd Rad 58: 299-303. doi: 10.1002/jlcr.3296

Zarschler K, Prapainop K, Mahon E, Rocks L, Bramini M, Kelly PM, Stephan H, Dawson KA (2014) Diagnostic nanoparticle targeting of the EGF-receptor in complex biological conditions using single-domain antibodies. Nanoscale 6: 6046-6056. doi: 10.1039/c4nr00595c